An Efficient Axi-symmetric Element Based on Inverse Approach for Cold Forging Modeling

Ali Halouani, Yuming Li, Boussad Abbès, Ying-Qiao Guo

Abstract— **This paper presents an efficient axi-symmetric finite element based on the "Inverse Approach" for the numerical modeling of cold forging process. In contrast to the classical incremental methods, the Inverse Approach exploits the known shape of the final part and executes the calculation from the final part to the initial billet. The assumptions of the proportional loading and the simplified tool actions make the I.A. calculation very fast. The formulation of an axi-symmetric element based on the I.A. is presented. The metal's incompressibility is ensured by the penalty method. The comparison with the simulation by Abaqus® shows the efficiency and limitations of the I.A. This kind of modeling will be a good tool for the preliminary preform design.**

Index Terms— **Cold forging process, large logarithmic strains, integrated constitutive law, axi-symmetrical element, Inverse Approach.**

I. INTRODUCTION

In a cold forging process, the metal is largely deformed under the tool actions. The forging process allows not only to change the billet's shape but also to improve the metal properties because it refines the metal grain sizes. Forged parts are often used for high performance and high reliability applications where the strength and the human safety are crucially important.

The numerical modeling plays an important role in the tool design for the forging process. Many research groups work on the forward method or on the backward tracing method for the forging simulation and optimization [1]-[7]. Very advanced works have been done by Chenot, Fourment et al. from CEMEF in France and the corresponding software FORGE is largely used in the forging industry.

Two simplified methods called Inverse Approach (I.A.) and Pseudo Inverse Approach (P.I.A.) have been developed by Batoz, Guo et al. [8], [9] for the sheet forming modeling. These approaches are less accurate but much faster than classical incremental approaches.

Manuscript received September 27, 2010. This work was supported by the French State and Champagne-Ardenne Region. The sponsors and financial support are gratefully acknowledged.

A. Halouani is in the Group of Research in Engineering Sciences (GRESPI), University of Reims Champagne-Ardenne, F51687 Reims, France (e-mail: ali.halouani@etudiant.univ-reims.fr).

Y.M. Li is in GRESPI, University of Reims Champagne-Ardenne, F51687 Reims, France (e-mail: yuming.li@univ-reims.fr).

B. Abbès is in GRESPI, University of Reims Champagne-Ardenne, F51687 Reims, France (corresponding author, phone: 33-3-26918135; fax: 33-3-26913803; email: boussad.abbes@univ-reims.fr).

Y.Q Guo is in GRESPI, University of Reims Champagne-Ardenne, F51687 Reims, France (email: yq.guo@univ-reims.fr).

The aim of the present work is to study the feasibility of the I.A. for the cold forging modeling [10]. The formulation of an axi-symmetric element based on the I.A. is developed for the preliminary preform design and optimization.

In this study, firstly, we present the basic idea of the I.A. and the main steps of the modeling. Then, we detail the formulation of an axi-symmetric element based on the I.A.: the principle of virtual work in large deformation, the definition of large logarithmic strains, the integrated constitutive law based on the assumption of proportional loading, the technique to ensure the incompressibility of the metal and the special treatment of the boundary conditions. Two examples will be presented to show the efficiency and limitations of the present I.A. for the forging process modeling.

II. OUTLINE OF THE INVERSE APPROACH

The Inverse Approach is based on the knowledge of the final part shape. The prediction of the trajectories of all material points from the initial billet to the known final part is done in one step by comparing directly the initial and final configurations. Two basic assumptions are used in this study: the assumption of proportional loading (for cold forging) gives an integrated constitutive law without considering the strain path and the visco-plasticity, and the assumption of contact between the part and tools allows one to replace the tool actions by nodal forces without contact treatment. These two assumptions make the I.A. calculation very fast.

The I.A. procedure is carried out as follows (Fig. 1):

1) The finite element mesh is created on the known final part.

2) As an initial solution, the nodes at the part contour are mapped on the known contour of the initial billet and a linear resolution allows determining the positions of the internal nodes in the initial billet.

3) The large logarithmic strains are calculated by using the Cauchy-Green left tensor between the two meshes, and the stresses are obtained by using an integrated constitutive law.

4) The metal's incompressibility is ensured by the penalty method.

5) An implicit Newton–Raphson algorithm is used to move the nodes in the initial billet in order to satisfy equilibrium in the final part.

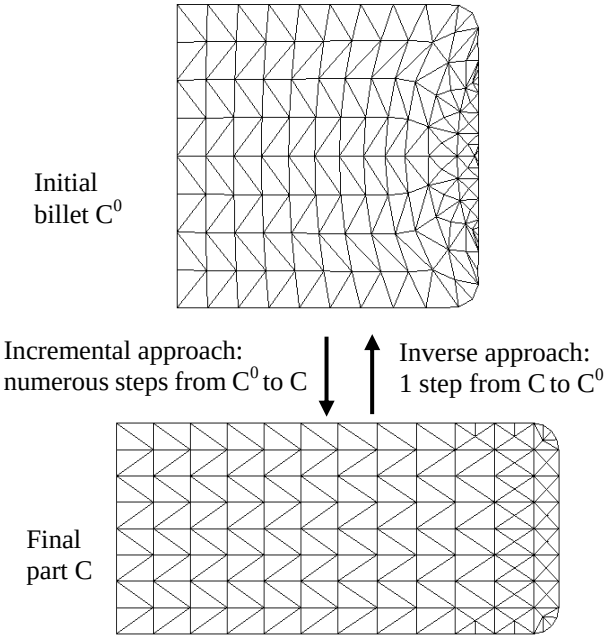

Fig. 1 Two approaches for forging process modeling

III. AXI-SYMMETRIC ELEMENT BASED ON I.A.

A. Principle of Virtual Work (PVW)

By contrast to incremental approaches, in the Inverse Approach, the final configuration is known and taken as the reference configuration. The equilibrium of the final part is expressed by the principle of virtual work which makes the finite element formulation much simpler:

$$W = \sum_{elt} W^e = \sum_{elt} \left(W^e_{\text{int}} - W^e_{\text{ext}} \right) = 0 \tag{1}$$

with $$W^e_{\text{int}} = \int_{v^e} \left\langle \varepsilon^* \right\rangle \{\sigma\}\, dv \tag{2}$$

$$W^e_{\text{ext}} = \int_{v^e} \left\langle u^* \right\rangle \{f\}\, dv \tag{3}$$

$$\langle \sigma \rangle = \langle \sigma_x \quad \sigma_\theta \quad \sigma_z \quad \sigma_{xz} \rangle$$

$$\left\langle \varepsilon^* \right\rangle = \left\langle \varepsilon^*_x \quad \varepsilon^*_\theta \quad \varepsilon^*_z \quad \gamma^*_{rz} \right\rangle$$

where W^e_{int} and W^e_{ext} are the element internal and external virtual works, $\langle \sigma \rangle$ the Cauchy stresses, $\left\langle \varepsilon^* \right\rangle$ the virtual strains, $\left\langle u^* \right\rangle$ the virtual displacements, $\{f\}$ the volume forces (including also other concentrated or distributed forces).

It is well to note that the virtual strains are infinitesimal, so they are linear functions of virtual displacements; whereas, the above Cauchy stresses are related to the large strains, so generally they are calculated by an incremental algorithm. In the present study, a total method is proposed:

1) The deformation gradient tensor and the Cauchy-Green left tensor are defined between the initial and final configurations.

2) Then, the principal elongations and large logarithmic strains are calculated.

3) Finally, the Cauchy stresses are calculated by using an integrated constitutive law based on the assumption of proportional loading.

B. Virtual strain operator

For an axi-symmetrical problem, the virtual strains in the global cylindrical coordinate system ($r\theta Z$) are written as follows (Fig. 2):

$$\left\{ \varepsilon^* \right\} = \begin{Bmatrix} U^*_{,r} \\ \dfrac{U^*}{r} \\ W^*_{,Z} \\ U^*_{,Z} + W^*_{,r} \end{Bmatrix} \tag{4}$$

where r is the radial coordinate, U^* and W^* are the virtual displacements in the radial direction $\boldsymbol{r}$ and the vertical direction $\boldsymbol{Z}$.

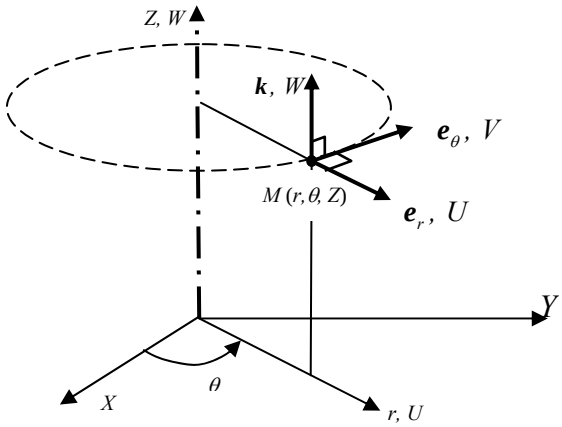

Fig. 2 Cylindrical coordinate system (r, θ, Z)

In our finite element formulation, it is more convenient to define the strains in the element local system ($x\theta z$) (Fig. 3):

$$\left\{ \varepsilon^* \right\} = \begin{Bmatrix} \varepsilon^*_x \\ \varepsilon^*_\theta \\ \varepsilon^*_z \\ \gamma^*_{xz} \end{Bmatrix} = \begin{Bmatrix} u^*_{,x} \\ \dfrac{U^*}{r} \\ w^*_{,z} \\ u^*_{,z} + w^*_{,x} \end{Bmatrix} = \begin{Bmatrix} u^*_{,x} \\ \dfrac{u^* \cos\alpha - w^* \sin\alpha}{r} \\ w^*_{,z} \\ u^*_{,z} + w^*_{,x} \end{Bmatrix} \tag{5}$$

where u^* and w^* are the virtual displacements along x and z, $\alpha = \alpha(\boldsymbol{r}, \boldsymbol{x})$ is the inclination angle of the local axis $\boldsymbol{x}$ with respect to the horizontal global axis $\boldsymbol{r}$.

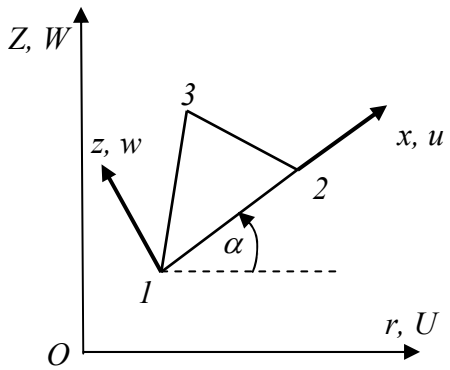

Fig. 3 Local ($x\theta z$) and global ($r\theta Z$) cylindrical coordinates

The proposed element is an axi-symmetrical CST element with three nodes and six degrees of freedom. The displacements are interpolated linearly in terms of nodal displacements**:**

$$\begin{Bmatrix} u \\ w \end{Bmatrix} = \begin{bmatrix} N_1 & 0 & N_2 & 0 & N_3 & 0 \\ 0 & N_1 & 0 & N_2 & 0 & N_3 \end{bmatrix} \{u_n\} \tag{6}$$

$$\{u_n\} = \langle u_1 \quad w_1 \quad u_2 \quad w_2 \quad u_3 \quad w_3 \rangle^T$$

where $N_i(x, z)$ are the classical linear interpolation functions for an element [11].

Substituting (5) into (4), we obtain the following virtual strain operator $[B_m]$:

$$\{\varepsilon^*\} = [B_m]\{u_n^*\} \tag{7}$$

with

$$[B_m] = \begin{bmatrix} N_{1,x} & 0 & N_{2,x} & 0 & N_{3,x} & 0 \\ \dfrac{N_1 \cos\alpha}{r} & -\dfrac{N_1 \sin\alpha}{r} & \dfrac{N_2 \cos\alpha}{r} & -\dfrac{N_2 \sin\alpha}{r} & \dfrac{N_3 \cos\alpha}{r} & -\dfrac{N_3 \sin\alpha}{r} \\ 0 & N_{1,z} & 0 & N_{2,z} & 0 & N_{3,z} \\ N_{1,z} & N_{1,x} & N_{2,z} & N_{2,x} & N_{3,z} & N_{3,x} \end{bmatrix} \tag{8}$$

C. Internal force vector

Substituting (7) into (2) gives the element internal force vector in the local element reference:

$$W_{\text{int}}{}^e = \langle u_n^* \rangle 2\pi \iint_{A^e} [B_m]^T \{\sigma\} r dA = \langle u_n^* \rangle \{F_{\text{int}}{}^e\} \tag{9}$$

Since the term $\{\sigma\} r$ depends on r, generally we should introduce the reference element and use the numerical integration to calculate the internal force vector in the local reference. A reduced integration method is proposed by Batoz and Dhatt [11]: the stresses are supposed constant in an element and the barycenter is taken as a single integration point for this linear function. Thus the calculation of the internal force vector becomes very simple:

$$\{F_{\text{int}}{}^e\} = 2\pi A r_m [B_m]^T_{r=r_m} \{\sigma\} \tag{10}$$

with: $r = r_{\text{m}} = \dfrac{1}{3}(r_1 + r_2 + r_3)$

D. External force vector

In a forging process, the initial billet is submitted to a normal pressure force and a tangential friction force on the contour. In the Inverse Approach, these tool actions are simply represented by some external nodal forces at the final configuration to avoid the contact treatment. At a node, the value of the resultant force is unknown; and the direction of this force $\boldsymbol{n_f}$ can be determined by the friction cone and the slide direction (Fig. 4):

$$\boldsymbol{n_f} = \frac{1}{\sqrt{1+\mu^2}}(\boldsymbol{n} - \mu \boldsymbol{t}) \quad ; \quad \mu = tan\beta \tag{11}$$

where $\boldsymbol{n}$ is the unit normal vector of the contour, $\boldsymbol{t}$ the unit tangent direction of the contour, μ the friction coefficient.

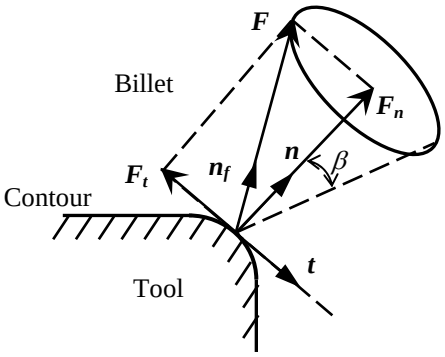

Fig. 4 Tool force direction determined by friction cone

The values of the tool action forces can be determined by the equilibrium condition at the contour. The FE discretization allows one to establish the following equations representing the equilibrium at a node k:

$$\{F_{ext}^k(P^k)\} - \{F_{\text{int}}^i\} = \begin{Bmatrix} P^k n_r^k \\ P^k n_Z^k \end{Bmatrix}_{ext} - \begin{Bmatrix} F_r^k \\ F_Z^k \end{Bmatrix}_{int} = \begin{Bmatrix} 0 \\ 0 \end{Bmatrix} \tag{12}$$

where $\langle n_r^k \quad n_Z^k \rangle^T = \boldsymbol{n_f}$ represents the direction of the resultant force at the node k, and $\{F_{\text{int}}^i\}$ the unknown internal force vector. The value of the resultant force P^k is then calculated by:

$$P^k = \langle n_r^k \quad n_Z^k \rangle \begin{Bmatrix} F_r^k \\ F_Z^k \end{Bmatrix}_{int} \tag{13}$$

The element external force vector is finally obtained:

$$\{F_{ext}^k\} = \langle n_r^k \quad n_Z^k \rangle \begin{Bmatrix} F_r^k \\ F_Z^k \end{Bmatrix}_{int} \begin{Bmatrix} n_r^k \\ n_Z^k \end{Bmatrix} \tag{14}$$

E. Inverse of deformation gradient tensor

In the Inverse Approach, we use an integrated constitutive law which associates the total strains to the total stresses. These large strains between the initial and final configurations are calculated by the following steps: the inverse of deformation gradient tensor ➔ the inverse of the Cauchy-Green left tensor ➔ the principal elongations ➔ the logarithmic strains.

The word « inverse » is used to indicate that the known final configuration is taken as the reference configuration, and the calculation is carried out from the known final part to the unknown initial billet.

The solid has an axis of revolution Z. A point M in the solid is defined in the global reference by its cylindrical coordinates (r, θ, Z) (Fig. 2). The displacement field is composed of the radial, circumferential and vertical displacements (U, V, W):

$$\boldsymbol{U} = U\boldsymbol{e}_r + V\boldsymbol{e}_\theta + Wk \tag{15}$$

The differential of the displacement field is given by:

$$d\boldsymbol{U} = (dU - Vd\theta)\boldsymbol{e}_r + (dV + Ud\theta)\boldsymbol{e}_\theta + dW\boldsymbol{k} \tag{16}$$

The above equation can be rewritten in the reference $(\boldsymbol{e}_r, \boldsymbol{e}_\theta, \boldsymbol{k})$ in a matrix form to define the displacement gradient tensor in cylindrical coordinates:

$$\begin{Bmatrix} dU \\ dV \\ dW \end{Bmatrix} = \begin{Bmatrix} dU - V d\theta \\ dV + U d\theta \\ dW \end{Bmatrix} = \begin{bmatrix} U_{,r} & U_{,\theta} - V & U_{,Z} \\ V_{,r} & V_{,\theta} + U & V_{,Z} \\ W_{,r} & W_{,\theta} & W_{,Z} \end{bmatrix} \begin{Bmatrix} dr \\ r d\theta \\ dZ \end{Bmatrix} \tag{17}$$

For an axi-symmetric problem, each point of the solid moves in its meridian plane ($V=0$) and the displacement field is independent of the circumferential coordinate ($\partial / \partial \theta = 0$). Thus, the displacement gradient tensor in cylindrical coordinates is reduced to:

$$\left[\frac{\partial \boldsymbol{U}}{\partial \boldsymbol{r}} \right] = \begin{bmatrix} U_{,r} & 0 & U_{,Z} \\ 0 & \dfrac{U}{r} & 0 \\ W_{,r} & 0 & W_{,Z} \end{bmatrix} \tag{18}$$

In our Inverse Approach in large strain and plasticity, it is more convenient to define the displacement gradient tensor in the element local system. It is easy to demonstrate that:

$$\begin{aligned} \left[\frac{\partial \boldsymbol{U}}{\partial \boldsymbol{r}} \right] &= \left[\frac{\partial \boldsymbol{U}}{\partial \boldsymbol{x}} \right] \left[\frac{\partial \boldsymbol{x}}{\partial \boldsymbol{r}} \right] = \left[\frac{\partial \left([T]^T \{\boldsymbol{u}\} \right)}{\partial \boldsymbol{x}} \right] \left[\frac{\partial \boldsymbol{x}}{\partial \boldsymbol{r}} \right] \\ &= [T]^T \left[\frac{\partial \boldsymbol{u}}{\partial \boldsymbol{x}} \right] [T] \end{aligned} \tag{19}$$

with $[T] = \begin{bmatrix} \cos\alpha & 0 & \sin\alpha \\ 0 & 1 & 0 \\ -\sin\alpha & 0 & \cos\alpha \end{bmatrix}$; $\alpha = \alpha(\boldsymbol{r}, \boldsymbol{x})$

and $\left[\dfrac{\partial \boldsymbol{u}}{\partial \boldsymbol{x}} \right] = \begin{bmatrix} u_{,x} & 0 & u_{,z} \\ 0 & \dfrac{u\cos\alpha - w\sin\alpha}{r} & 0 \\ w_{,x} & 0 & w_{,z} \end{bmatrix}$

where $[T]$ is the transformation matrix between the global and local coordinate systems.

Now we consider the movement of a material point $\boldsymbol{x}^0 = \boldsymbol{x} - \boldsymbol{u}$, where $\boldsymbol{x}^0$ and $\boldsymbol{x}$ are the initial and final position vectors, $\boldsymbol{u}$ is the displacement vector in the local reference from $\boldsymbol{x}^0$ to $\boldsymbol{x}$. Then the inverse of the deformation gradient tensor is defined as follows:

$$\{d\boldsymbol{x}^0\} = \left[\frac{\partial \boldsymbol{x}^0}{\partial \boldsymbol{x}} \right] \{d\boldsymbol{x}\} = \left([I] - \left[\frac{\partial \boldsymbol{u}}{\partial \boldsymbol{x}} \right] \right) \{d\boldsymbol{x}\} = [F]_l^{-1} \{d\boldsymbol{x}\} \tag{20}$$

$$[F]_l^{-1} = \begin{bmatrix} 1 - u_{,x} & 0 & -u_{,z} \\ 0 & 1 - \dfrac{u\cos\alpha - w\sin\alpha}{r} & 0 \\ -w_{,x} & 0 & 1 - w_{,z} \end{bmatrix} \tag{21}$$

F. Cauchy-Green left tensor and large logarithmic strains

The inverse of the Cauchy-Green left tensor in the local reference is defined by the following expressions:

$$\langle d\boldsymbol{x}^0 \rangle \{d\boldsymbol{x}^0\} = \langle d\boldsymbol{x} \rangle [F]_l^{-T} [F]_l^{-1} \{d\boldsymbol{x}\} = \langle d\boldsymbol{x} \rangle [B]^{-1} \{d\boldsymbol{x}\} \tag{22}$$

with $[B]^{-1} = [F]_l^{-T} [F]_l^{-1} = \begin{bmatrix} a & 0 & b \\ 0 & d & 0 \\ b & 0 & c \end{bmatrix}$

where:

$a = (1 - u_{,r})^2 + w_{,r}^2$

$b = -u_{,z}(1 - u_{,r}) - w_{,r}(1 - w_{,z})$

$c = (1 - w_{,z})^2 + u_{,z}^2$

$d = \left(1 - \dfrac{u\cos\alpha - w\sin\alpha}{r}\right)^2$

The tensor $[B]^{-1}$ defined in the local reference can be transformed to the principal reference to obtain the three eigenvalues $(\lambda_1^{-2}, \lambda_2^{-2}, \lambda_3^{-2})$, then the three principal elongations $(\lambda_1, \lambda_2, \lambda_3)$:

$$[B]^{-1} = [M] \begin{bmatrix} \lambda_1^{-2} & 0 & 0 \\ 0 & \lambda_2^{-2} & 0 \\ 0 & 0 & \lambda_3^{-2} \end{bmatrix} [M]^T \tag{23}$$

with $\begin{Bmatrix} \lambda_1^{-2} \\ \lambda_3^{-2} \end{Bmatrix} = \left\{ \dfrac{a+c}{2} \pm \sqrt{\left(\dfrac{a-c}{2} \right)^2 + b^2} \right\}$ (24)

$$[M] = \begin{bmatrix} \cos\varphi & 0 & -\sin\varphi \\ 0 & 1 & 0 \\ \sin\varphi & 0 & \cos\varphi \end{bmatrix} \tag{25}$$

where φ is the angle from the local reference to the principal reference.

Finally, the principal logarithmic strains are obtained:

$$\{\varepsilon\} = \begin{Bmatrix} \varepsilon_1 \\ \varepsilon_2 \\ \varepsilon_3 \end{Bmatrix} = \begin{Bmatrix} Log\,\lambda_1 \\ Log\,\lambda_2 \\ Log\,\lambda_3 \end{Bmatrix} \tag{26}$$

The large logarithmic strains in the local reference can be obtained by the following transformation:

$$\{\varepsilon_l\} = \begin{Bmatrix} \varepsilon_x \\ \varepsilon_\theta \\ \varepsilon_z \\ \gamma_{xz} \end{Bmatrix} = \begin{bmatrix} \cos^2\varphi & 0 & \sin^2\varphi \\ 0 & 1 & 0 \\ \sin^2\varphi & 0 & \cos^2\varphi \\ 2\sin\varphi\cos\varphi & 0 & -2\sin\varphi\cos\varphi \end{bmatrix} \begin{Bmatrix} \varepsilon_1 \\ \varepsilon_2 \\ \varepsilon_3 \end{Bmatrix} \tag{27}$$

The assumption of incompressibility of the metal leads to the null volume strain:

$$\varepsilon_v = \varepsilon_1 + \varepsilon_2 + \varepsilon_3 = \varepsilon_x + \varepsilon_\theta + \varepsilon_z = 0 \tag{28}$$

$$\lambda_1 \lambda_2 \lambda_3 = \lambda_x \lambda_\theta \lambda_z = 1 \tag{29}$$

G. Penalization method for metal incompressibility

The incompressibility of the metal can be ensured by introducing a Lagrange multiplier or a penalization term (Kobayashi and Altan [2]). In our Inverse Approach, we add a penalization term in the Principle of Virtual Work:

$$W = \sum_{elt} \left(\int_{v^e} \langle \varepsilon^* \rangle \{\sigma\}\, dv - \int_{v^e} \langle u^* \rangle \{f\}\, dv + \int_{v^e} K \varepsilon_v^* \varepsilon_v\, dv \right) = 0 \tag{30}$$

where ε_v is the volume strain, K is a great positive factor which allows to annul ε_v in the convergence loop. Using the virtual strains operator (8), we obtain a vector of "equivalent forces" relative to the volume stain:

$$\varepsilon_v^* = \langle u_n^* \rangle [B_m]_{6\times 3}^T \begin{Bmatrix} 1 \\ 1 \\ 1 \end{Bmatrix} = \langle u_n^* \rangle \{B_v\} \tag{31}$$

$$\text{with} \quad \int_{v^e} K \ \varepsilon_v^* \ \varepsilon_v \ dv = \langle u_n^* \rangle \{ F_v^e \} \tag{32}$$

We finally obtain:

$$\{ F_v^e \} = 2\pi r_m A K \{ B_v \}_{r_m} (\varepsilon_x + \varepsilon_\theta + \varepsilon_z) \tag{33}$$

H. Integrated constitutive law (Hencky-Mises)

In the present study, the isotropic constitutive law is adopted. The Von Mises criterion of plasticity is expressed by:

$$f = \bar{\sigma} - \sigma_Y = (\langle \sigma \rangle [P] \{\sigma\})^{\frac{1}{2}} - \sigma_Y = 0 \tag{34}$$

$$\text{with} \ \bar{\sigma} = \frac{\sqrt{2}}{2} \left[(\sigma_x - \sigma_\theta)^2 + (\sigma_\theta - \sigma_z)^2 + (\sigma_z - \sigma_x)^2 + 6\sigma_{xz}^{\ 2} \right]^{\frac{1}{2}}$$

where $\bar{\sigma}$ is the equivalent stress, σ_Y is the yield stress.

The normality law allows us to establish the relation between the plastic strain rate and the Cauchy stress using the plastic multiplier $\dot{\lambda}$:

$$\{ \dot{\varepsilon}^p \} = \dot{\lambda} \frac{\partial f}{\partial \{\sigma\}} = \frac{\dot{\lambda}}{\bar{\sigma}} [P] \{ \sigma \} \tag{35}$$

$$\text{Then} \quad \dot{\bar{\varepsilon}}^p = (\langle \dot{\varepsilon}^p \rangle [P]^{-1} \{ \dot{\varepsilon}^p \})^{\frac{1}{2}} = \dot{\lambda} \tag{36}$$

Using (34) to (36), we obtain:

$$\{ \dot{\varepsilon}^p \} = \frac{\dot{\bar{\varepsilon}}^p}{\bar{\sigma}} [P] \{\sigma\} \tag{37}$$

The assumption of proportional loading allows to analytically integrating the plastic strain rate:

$$\begin{aligned} \{ \varepsilon^p \} = \int_0^t \{ \dot{\varepsilon}^p \} dt &= \frac{\bar{\varepsilon}^p}{\bar{\sigma}} [P] \{\sigma\} \\ &= \frac{1}{H_s} [P] \{\sigma\} = (\frac{1}{E_s} - \frac{1}{E}) [P] \{\sigma\} \end{aligned} \tag{38}$$

where $E_s = \dfrac{\bar{\sigma}}{\bar{\varepsilon}}$ is the secant modulus of the uniaxial stress–strain curve (Fig. 5).

Adding the elastic strains to the plastic strains of (38), we obtain the total strain:

$$\{\varepsilon\} = \{ \varepsilon^p \} + \{ \varepsilon^e \} = ([C] + (\frac{1}{E_s} - \frac{1}{E}) [P]) \{\sigma\} \tag{39}$$

where $[C]$ is the elastic flexibility matrix.

Finally, the total Cauchy stresses are obtained in terms of the total logarithmic strains as:

$$\{ \sigma \} = [H_{ep}] \{\varepsilon\} = ([C] + (\frac{1}{E_s} - \frac{1}{E}) [P])^{-1} \{\varepsilon\} \tag{40}$$

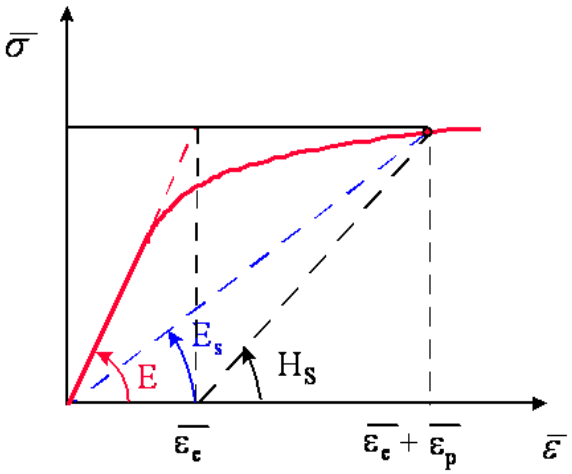

Fig. 5 Secant modulus of the uniaxial stress–strain curve

I. Boundary conditions on an irregular contour

In the present Inverse Approach, the displacements of the nodes on the contour are supposed tangential to the contour defined by the tools. Dhatt and Touzot [12] proposed to establish a contour reference and impose the null normal displacement in this reference.

Considering a node i on the contour of a mesh (Fig. 6). We establish a contour reference defined by the tangential and normal directions in which we impose the normal displacement $V_i' = 0$ (tangent displacement $U_i' \neq 0$). The following matrix allows one to transform the displacements between the contour reference and the global reference:

$$\begin{Bmatrix} U_i \\ V_i \end{Bmatrix} = \begin{bmatrix} \cos\alpha_i & -\sin\alpha_i \\ \sin\alpha_i & \cos\alpha_i \end{bmatrix} \begin{Bmatrix} U'_i \\ V'_i \end{Bmatrix} \tag{41}$$

It is more convenient to transform the tangent stiffness matrix and the vector of residual forces at the elementary level.

After the resolution, the displacements in the contour references ($U_i' \neq 0$, $V_i' = 0$) should be re-transformed into the global reference.

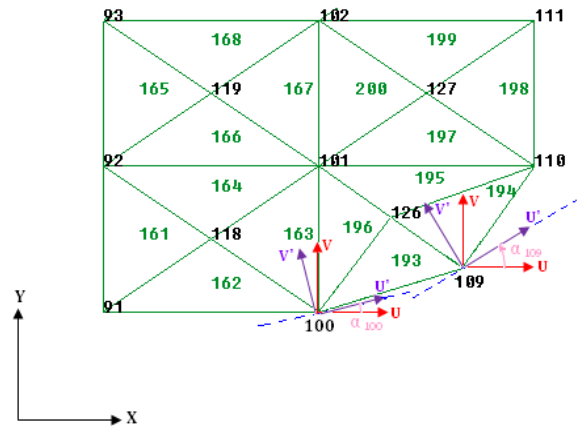

Fig. 6 Contour reference for boundary condition treatment

IV. NUMERICAL RESULTS

The validation of the simplified Inverse Approach is done by using the commercial code ABAQUS®/Explicit. Two axi-symmetric parts are considered.

A. Cold forging of a circular disc

The geometry of the circular disc is shown in Fig. 7. In the simulation by the Abaqus incremental approach, the initial billet is discretized into 1064 axi-symmetric triangle elements (CAX3 of Abaqus). The tools (punch and die) are supposed rigid and modeled by analytic rigid wires. The punch's displacement was specified by using a reference point on the punch. The total punch travel is 35.2 mm.

A master-slave contact method is used in this simulation where the tools are considered as the master surfaces and the outer surface of the billet (surface facing the tools) constitutes the slave surface.

The material properties of the billet are: Young's modulus E=10300 MPa, Poisson's ratio ν=0.3, friction coefficient μ=0.15, Hollomon stress-strain curve $\bar{\sigma}=567.29\left(\bar{\varepsilon}^{p}\right)^{0.26}$ MPa.

In order to compare the two approaches, we mesh the billet (Fig. 8a) and use Abaqus to obtain the mesh of the final part (Fig. 8b), then we use this mesh for I.A. modeling to obtain the mesh of the initial billet (Fig. 8c). We note that the mesh of the initial billet obtained by I.A. is very similar to that used for Abaqus simulation.

The distributions of the equivalent plastic strain obtained by the Inverse Approach and Abaqus are shown in Fig. 9. We note that the distributions are similar and the maximal and minimal values are in good agreement.

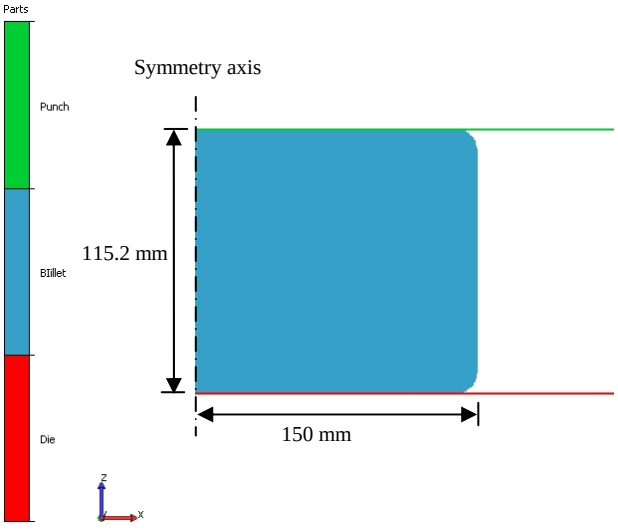

Fig. 7 Geometry of the circular disc

The CPU times for the modeling of the circular disc are compared: 233s are used by Abaqus incremental approach, only 9s are used by the Inverse Approach (a ratio of 25). The Inverse Approach is faster than the classical incremental approach.

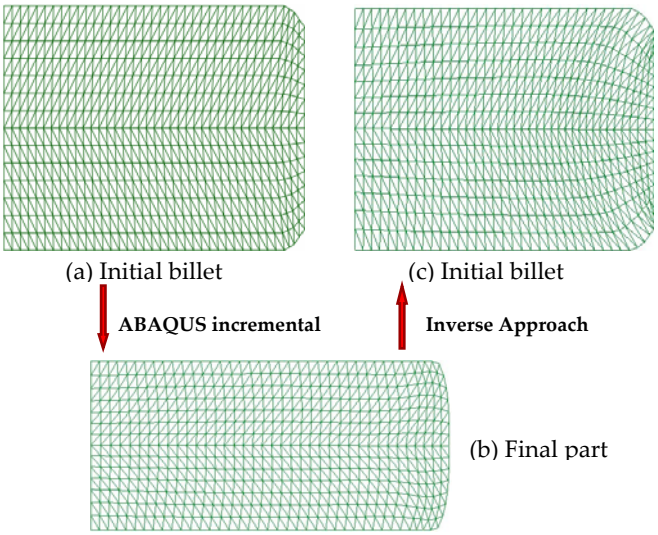

Fig. 8 Initial and final meshes of the part 1

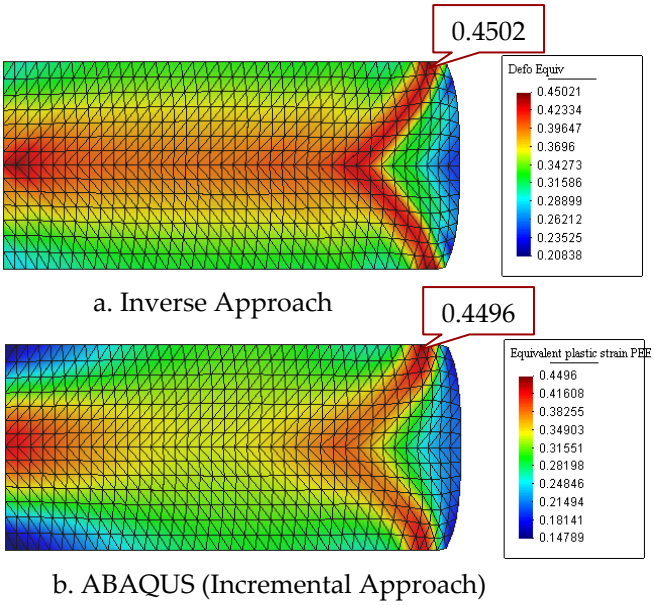

Fig. 9 Equivalent plastic strain obtained by I.A. and Abaqus

B. Cold forging of a wheel

The wheel (Fig. 10) has a horizontal plane of symmetry. The half section is meshed with 889 axi-symmetric triangle elements (CAX3 of Abaqus) (Fig. 11).

The material of the billet is the lead having the following properties: Young's modulus E=17 GPa, Poisson's ratio ν=0.42, friction coefficient μ=0.35, Hollomon stress-strain curve $\bar{\sigma}=65.8\left(\bar{\varepsilon}^{p}\right)^{0.27}$ MPa. The punch travel is 37.2 mm.

The mesh of the initial billet and the mesh of the final part obtained by Abaqus are shown by Fig. 11a and Fig. 11b. Then we use the mesh of Fig. 11b for the I.A. modeling which gives the mesh of the initial billet (Fig. 11c). A fairly good agreement is observed between the two meshes of the initial billet (Fig. 11a and Fig. 11c).

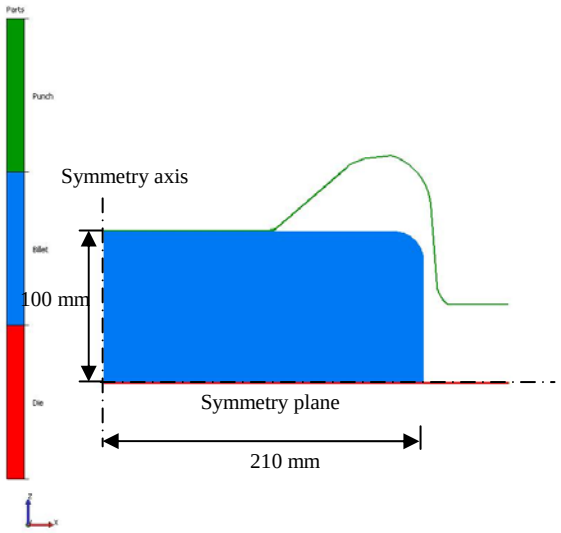

Fig. 10 Geometry of the wheel

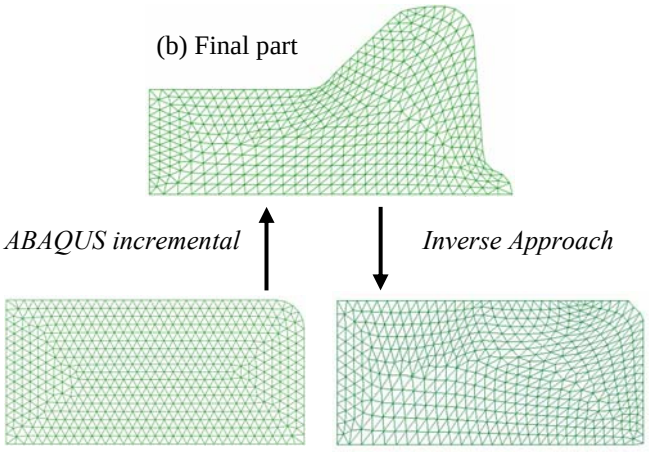

(a) Initial billet (c) Initial billet

Fig. 11 Initial and final meshes of the wheel

Fig. 12 shows the distributions of the equivalent plastic strain obtained by the Inverse Approach and Abaqus incremental approach. We observe that these strain distributions are quantitatively very close to each other. The maximum plastic equivalent strains are respectively 0.967 and 1.011. The error is reasonably acceptable (4.4%).

For the modeling of the wheel, the Inverse Approach has shown once again its efficiency compared to the incremental approach: 325s of CPU are used by ABAQUS incremental calculation, but only 54s are used by the Inverse Approach (a ratio of 6).

V. CONCLUSIONS

An efficient axi-symmetric element based on the "Inverse Approach" (I.A.) has been developed for the cold forging modeling. The approach exploits at the maximum the knowledge of the shape of the final part. The assumptions of the proportional loading and the simplified tool actions make the I.A. simulation very fast.

The equivalent plastic strain distribution obtained by the Inverse Approach is very close to that obtained by the Abaqus incremental approach. The Inverse Approach is very advantageous to quickly realize the preliminary perform design and optimize the process parameters.

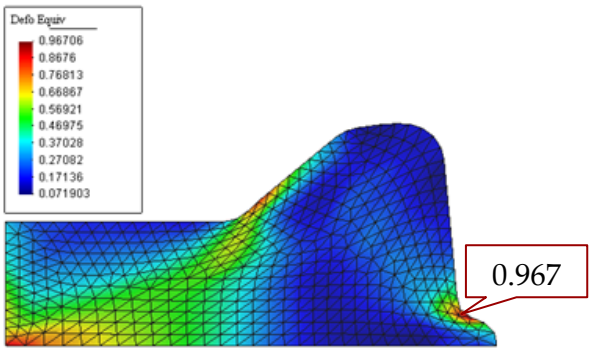

(a) Inverse Approach (1 step)

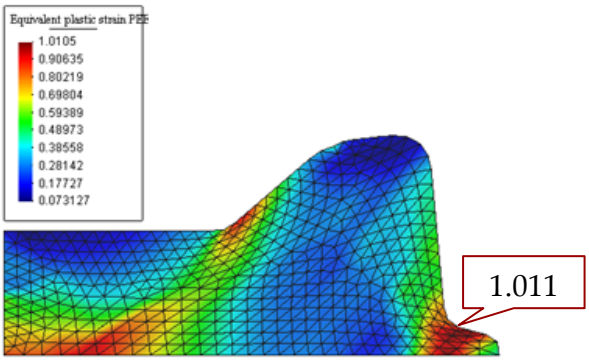

(b) ABAQUS Incremental Approach (150 steps)

Fig. 12 Equivalent plastic strain obtained by I.A. and Abaqus

Some limitations of the I.A. are also observed. The assumptions on the constitutive law and the tool actions are questionable; they cannot provide good stress estimation because of neglecting the loading history. For complex parts in very large strains, the remeshing operation and a more powerful resolution algorithm should be considered.

The future work for the forging modeling is to improve the stress estimation. Recently, a new approach called "Pseudo Inverse Approach" (P.I.A.)has already been proposed by Guo et al. [9], [13] for the sheet forming modeling, which keeps the advantages of the I.A. but gives good stress estimation with the loading history consideration. This new P.I.A. will be adapted for the forging applications.

ACKNOWLEDGMENTS

The financial support of the French State and the Champagne-Ardenne Region is gratefully acknowledged. We also thank the laboratory LASMIS of the University of Technology of Troyes for the fruitful discussions and collaboration.

REFERENCES

[1] C. Bohatier, J. L. Chenot, "Finite element formulation for non steady state viscoplastic deformation", *Int. J. Meth. Eng.*, vol. 21, 1985, pp. 1697-1708.

[2] S. Kobayashi , S. I. Oh, T. Altan, *Metal forming and finite element method*, Oxford University Press, 1989.

[3] G. Zhao, E. Wright, R. V. Grandhi, "Forging perform design with shape complexity control in simulating backward deformation", *Int. J. Mach. Manuf.*, vol. 359, 1995, pp. 1225-1239.

[4] L. Fourment, S. H. Chung, "Direct and adjoint differentiation methods for shape optimization in non-steady forming application", *European Conference on Computational Mechanics*, Cracow, 2001.

[5] T. Altan, G. Ngaile, G. Shen, *Cold and hot forging – Fundamentals and Applications*, ASM International Materials Park, Ohio, 2007.
[6] G. W. Rowe, C. E. N. Sturgess, P. Hartley, I. Pillinger, *Finite – element plasticity and metal forming analysis*, Cambridge University Press, 2005.
[7] R. H. Wagoner, J. L. Chenot, *Metal forming analysis*, Cambridge University Press, 2005.
[8] Y. Q. Guo, J. L. Batoz, J. M. Detraux, P. Duroux, "Finite element procedures for strain estimations of sheet metal forming parts", *Int. J. Num. Meth. Eng*., vol. 30, 1990, pp. 1385-1401.
[9] W. Gati, Y. Q. Guo, H. Naceur, J. L. Batoz, "Approche pseudo-inverse pour estimation des contraintes dans les pièces embouties axisymétriques", *Revue Européenne des Eléments Finis*, vol. 12(7-8), 2003, pp. 863-886.
[10] A. Halouani, Y. M. Li, B. Abbès, Y. Q. Guo, "An axisymmetric Inverse Approach for cold forging modelling", Lecture Notes in Engineering and Computer Science: Proceedings of The World Congress on Engineering 2010, WCE 2010, 30 June - 2 July, 2010, London, U.K., pp.1230-1235.
[11] G. Dhatt, G. Touzot, *Une présentation de la méthode des éléments finis*, Maloine S.A. Editor, Paris, 1984.
[12] J. L. Batoz, G. Dhatt, *Modélisation des structures par éléments fini*, Vol. 1, *Solides élastiques*, HERMES, Paris, 1990.
[13] Y. Q. Guo, Y. M. Li, F. Bogard and K. Debray, "An efficient pseudo-inverse approach for damage modeling in the sheet forming process", *J. Mater. Proc. Technol.*, vol. 151(1-3), 2004, pp. 88-97.